ELSEVIER

Polymer 43 (2002) 4153–4157

polymer

www.elsevier.com/locate/polymer

Polyamide membrane precipitation studied by confocal backscattering microscopy

James L. Thomas*, Martina Olzog, Christin Drake, Chien-Hsieh Shih, Carl C. Gryte

Department of Chemical Engineering and Applied Chemistry, Columbia University, 500 W. 12th Street, New York, NY 10027, USA

Received 15 January 2002; received in revised form 29 March 2002; accepted 1 April 2002

Abstract

A wide variety of commercial polymeric membranes are manufactured by a non-solvent immersion precipitation process, yet the detailed mechanism and kinetics of membrane formation are poorly understood. We have used a confocal microscope, with fluorescence filters removed, to observe backscatter from precipitating nylon 6 films. Nylon 6 in formic acid/water solutions was spread on a glass substrate, which was then quickly immersed into water or water/formic acid non-solvent baths. Two slope-casting chambers were designed in order to observe the precipitation process from both the substrate side and the bath side (in separate experiments). From the substrate side, a scattering front was observed to form within a few seconds after immersion, and then to progress toward the substrate as the precipitated film formed. When observed from the bath side, the scattering front first moved toward the bath for approximately 5–10 s, then reversed direction and moved toward the substrate. This later motion toward the substrate can be explained by the contraction of the film as water is expelled. The initial motion toward the bath implies that the initial point of precipitation is not at the film surface, but rather at some depth (ca. 60 + μm) within the film. This new application of confocal microscopy has enabled measurements of the dynamics of nylon membrane precipitation with sufficient time and depth resolution to permit quantitative testing of models of the precipitation process. © 2002 Published by Elsevier Science Ltd.

Keywords: Polyamide membranes; Confocal microscopy; Immersion precipitation

1. Introduction

Commercial microporous membranes are often manufactured by a 'phase inversion' process, in which a homogeneous polymer solution is induced to phase separate into polymer-rich and polymer-poor phases. The polymer-rich phase eventually forms the matrix, while the polymer-poor phase forms the membrane pores. Commonly, the phase separation is induced by immersion precipitation, in which a polymer solution is cast onto a support and then immersed into a coagulating non-solvent bath. The rapid diffusive efflux of solvent and influx of non-solvent quickly leads to the formation of a precipitated membrane. This process can involve liquid–liquid phase separation (either binodal or spinodal) and, in the case of aliphatic polyamides, polymer crystallization [1]. The phase transition kinetics can affect which of the mechanisms is operative, and can consequently control the morphology and barrier properties of the resultant membrane.

Because the immersion precipitation membranes are inhomogeneous on the length scale of the wavelength of light, they scatter light effectively, and are opaque even at thicknesses of less than 100 μm. Consequently, optical techniques have been successfully applied to study the kinetics of membrane formation. In particular, optical transmission after immersion has been used to measure the lag time to initial precipitation [2]. Diffusive modeling of solvent and non-solvent fluxes after immersion suggested that the lag may be associated with the time required for the sample to reach spinodal composition. However, further experiments and experimental techniques will be necessary to fully elaborate the respective roles of the different phase separation mechanisms.

Clearly, a more detailed picture of the film profile during the precipitation process would be helpful in elucidating precipitation mechanisms. Toward that end, we have used a confocal fluorescence microscope to study the spatial progress of the precipitation event as it proceeds through the nascent film. To observe backscatter, rather than fluorescence, we simply removed the barrier filters that block the incident wavelength. Backscatter has been used in the biomedical field to image samples using confocal microscopy [3,4], but this is the first application of the technique

* Corresponding author. Tel.: +1-212-854-8632; fax: +1-212-854-3054.
E-mail address: jlt32@columbia.edu (J.L. Thomas).

0032-3861/02/$ - see front matter © 2002 Published by Elsevier Science Ltd.
PII: S0032-3861(02)00250-1

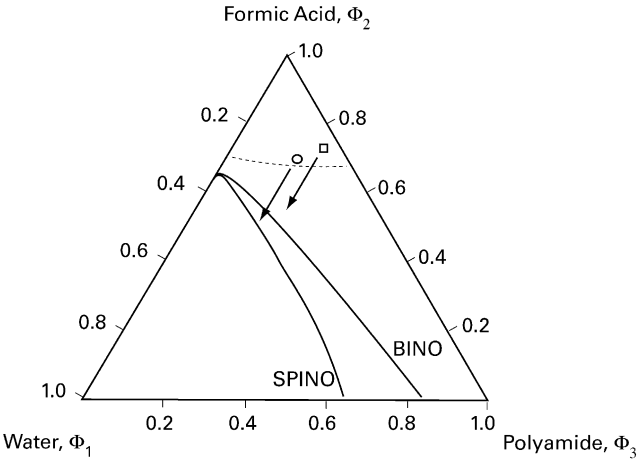

Fig. 1. Ternary phase diagram of the polyamide/water/formic acid system at 25 °C, from Shih [5]. The starting dopes are shown as the circle (dope A) and the square (dope B). Immersion into the non-solvent moves the composition of the film in the approximate direction of the arrows, through water–formic acid diffusional exchange. (Polymer concentration is also expected to increase, owing to a more rapid efflux of formic acid than influx of water; a mathematical analysis based on a layer model is presented in Shih [5].) The approximate location of the crystallization phase boundary is shown as the dashed line; the binodal (BINO) and spinodal (SPINO) phase boundaries are indicated.

to observe polymer membrane immersion precipitation, to our knowledge. In order to obtain relatively fast kinetic information, the precipitating sample was held at a fixed angle with respect to the horizontal; a 'line scan' then probes different depths in the sample at different x positions. Using this approach, the kinetics of membrane formation was observed, and for the first time, the scattering profile through the sample was determined. The most significant observation is that the precipitation occurs *first* at a significant depth, and then propagates *both* upward and downward through the polymer film.

2. Experimental

2.1. Polymer solutions

The polyamide nylon 6 (Zytel 211, DuPont, $[\eta] = 1.845$ dl/g) was prepared in formic acid/water solvent solutions. Volume fractions of each component were $\Phi_1 = 0.04$, $\Phi_2 = 0.73$, $\Phi_3 = 0.23$ (dope A; $1, 2, 3 =$ water, formic acid, and nylon, respectively) or $\Phi_1 = 0.115$, $\Phi_2 = 0.7$, $\Phi_3 = 0.185$ (dope B). The starting compositions are shown in the ternary phase diagram, Fig. 1; dope B is closer to the crystallization line than dope A.

2.2. Slope-casting chamber

Two different 'slope-casting' chambers (R. Knight, personal communication) were designed to permit observation of film formation from the substrate side and from the bath side of the precipitating film (in separate experiments).

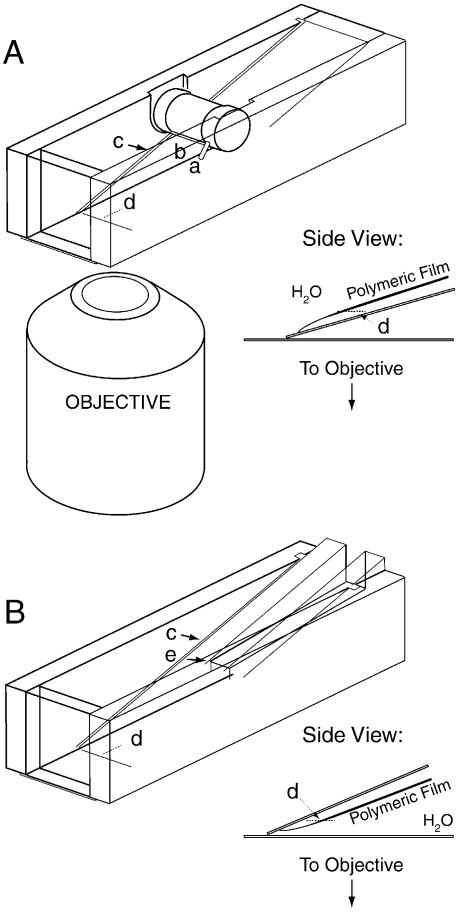

Fig. 2. The immersion chambers for (A) substrate-side viewing and (B) bath-side viewing. Channels 0.008 in. wide (c) guide a 24×50 mm microscope coverslip past a thickness-determining barrier and into the non-solvent bath. In (A), the pin (a) rotates the barrier bar as the coverslip is immersed, moving a dam (b). In (B), the shelf (e) determines the film thickness. The confocal microscope is programmed to take an x–t scan, along the scan line (d).

The chambers are shown in Fig. 2. The substrates were ordinary glass coverslips. A 24×50 mm microscope coverslip was slotted into 0.008 in. 'tracks' (guides) in the slope caster. An upper chamber on the slope caster held the polymer dope in contact with the coverslip, either on top of the coverslip (for viewing from the substrate side, Fig. 2(A)) or beneath it (for viewing from the bath side, Fig. 2(B)). For substrate-side viewing, manually pushing the coverslip down the sloping tracks rotated a cylindrical barrier (b) and allowed a thin liquid film to be spread over the coverslip surface as it became immersed in water (or a softer non-solvent bath) in the lower chamber; the film thickness was determined by the smaller diameter of the cylinder center. For bath-side viewing, a simpler chamber with a fixed gap (e) was used; the upper chamber was filled with polymer solution *immediately* prior to the experiment, and the relatively high viscosity of that solution prevented rapid leaking through the narrow gap. Experiments were done at room temperature (nominally 25 °C). The confocal

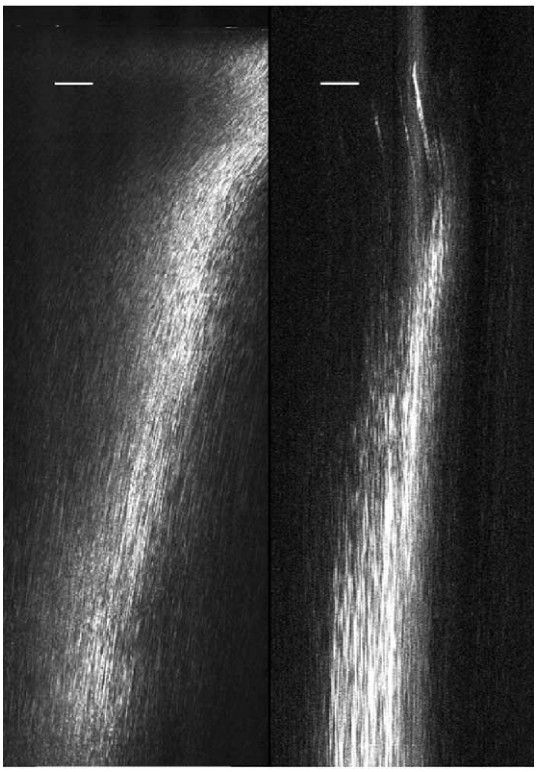

Fig. 3. x–t images of polymer membrane precipitation. The confocal microscope was used to take a sequence of line scans while a coverslip coated with polymer-solvent was rapidly immersed. The left image was taken with chamber A, which views the growing film from the substrate side. The scattering signal originates at the right edge of the image, higher in the polymer solution, and propagates downward, slowing somewhat after the initial 10–15 s. The right image was taken (in a separate experiment) with chamber B, which views the growing film from the bath side. The scattering first propagates *outward*, toward the bath; subsequently, there is an inward motion which is most likely caused by the contraction of the film as a whole. Bars = 100 μm in the x-direction. The vertical axis is time; the entire interval shown is 75 s.

microscope (Olympus Fluoview, on an Olympus IX70 inverted microscope), with fluorescence emission filters removed, was set to scan repeatedly in the direction of the slope caster gradient. Because of the left-to-right incline of the slope caster, the left end of the scan imaged deep within the sample (for bath-side imaging), while the right end imaged near the surface. An Olympus LC PlanFL 20× infinity-corrected long working distance objective with an numerical aperture (NA) of 0.40 was used. The 5 mW argon ion laser source was used ($\lambda = 488$ nm), with maximum attenuation (6% transmission). Each line scan took 0.1024 s, and covered a lateral (x) distance of 706 μm with 512 pixels/line.

2.3. Data analysis

Measurements were made directly on x–t scanned images using the Olympus Fluoview software. In some measurements, MatLab software was used to analyze the breadth of the precipitation front. Line scans were measured directly with Fluoview imaging software, then read into MatLab; fitting used the Levenberg–Marquardt algorithm (Matlab: LSQCURVEFIT) with a subroutine to compute the expected scattering profiles.

2.4. Electron microscopy

The preparation of membranes for electron microscopy has been described previously [2]. Briefly, fully precipitated membranes were dried, frozen in liquid nitrogen, and then fractured to expose a membrane cross-section. The membrane coated under vacuum with gold and palladium and viewed with a scanning electron microscope at 10 keV.

3. Results

Fig. 3 shows two typical immersion experiments. The time axis is vertical, and the x axes are horizontal. The left image was taken through the substrate, and is oriented such that the substrate would appear to the left of the image. Using a different slope caster, the right image was taken viewing the film from the bath side, with the same orientation (substrate to the left). The scale bars represent 100 μm of horizontal displacement; because of the differing tilts of the slope casters, this corresponds to a 28 μm displacement perpendicular to the film for the left image, and 52 μm for the right image. (The slope casters have slopes of 16 and 31.5°, respectively.) The samples were dope A, and were immersed into a pure water bath.

Several important qualitative features of the backscattering images are apparent. Viewed through the substrate, the scattering front advances down through the film, first quickly and then more slowly. At later times, the backscattering signal is obtained only from regions in the sample that are close to the glass substrate. This is caused by the opacification of the film, which prevents light from penetrating more than a few micrometers. Opacification was confirmed by measuring the transmitted light on the microscope: within 15–20 s after immersion, the transmitted signal falls to zero.

The scattering front in Fig. 3, left, is rather broad: ca. 200 μm in the x direction, corresponding to a displacement of approximately 55 μm perpendicular to the substrate. However, micrometer-thick fluorescent films, when scanned in the same geometry, yielded similarly broad profiles. Thus, the poor z-resolution is likely caused by the use of an objective with a low NA (0.4), necessitated by the long working distance required. The film profiles thus show that the scattering length within the precipitating film is less than 55 μm, though a more precise assessment cannot be made on the basis of observations reported here.

The images taken (in a separate experiment) from the bath side of the precipitating film are even more remarkable. In all cases, the precipitating front was first observed to move *toward* the bath, and then, after a delay of approximately 5–10 s, move back toward the substrate. The later

Table 1
Velocities of the substrate-moving scattering front

	Early velocity (μm/s)	Late velocity (μm/s)
Dope A ($n = 5$)	6.6 ± 1.2	1.5 ± 0.3
Dope B ($n = 4$)	8.0 ± 2.5	1.65 ± 0.2

motion toward the substrate likely represents contraction of the film as a whole, as formic acid diffuses outward. That such contraction occurs has been predicted from the diffusive fluxes of water and formic acid, and has also been experimentally verified by direct film thickness measurements [5]. The most natural interpretation of the earlier, outward-moving scattering front is that precipitation first occurs at some depth within the nylon-formic acid-rich layer, and then propagates both outward and inward as the film develops.

3.1. Velocities of scattering fronts

The average velocity of the scattering front, observed through the substrate, was measured at both short (5–15 s) and long times (15–35 s) after immersion, by measuring the position of the peak scattering intensity as a function of time. The results are shown in Table 1, interpreted as displacements perpendicular to the substrate. The velocities of the two different film compositions are equal, within experimental uncertainty. In electron micrographs (shown below), there is a 'skin' structure in these films that is caused by rapid vitrification at the interface between the polymer solution and the non-solvent bath [1,6]. The rate of propagation of the scattering front through the film may be dominated by the transport properties of this skin, obscuring small differences that might arise from the differing water contents of the two dopes.

Results from kinetic measurements on film precipitation observed from the bath side are shown in Table 2. There is considerable variation in the measured parameters, which may arise from the relatively uncontrolled immersion velocity in these experiments. In spite of the variation, it is apparent that dope B, containing a higher water content, proceeded through the precipitation process more rapidly, with both higher front velocities and more rapid turnaround time, t_{inv}. The distance traversed by the outward-moving front is shown in the fourth column, Δz, and was significantly larger for dope B than for dope A.

As shown in Table 3, clear systematic differences were seen when nylon 6 films were immersed in baths of differing formic acid contents. When a 73:23:4 formic acid/nylon/water dope was immersed into softer baths, the onset of precipitation became somewhat slower, as did the velocities of the precipitating front. These differences may reflect differences in the microstructure of the film skin, which undoubtedly affects transport processes in the nascent film. There is considerable evidence that softer baths produce a less compact membrane skin, and thus formic acid efflux may be facilitated [5].

Table 2
Velocities of the bath-observed scattering front. v_o is the outward velocity immediately after immersion, v_i is the inward velocity after 'turnaround', t_{inv} is the time of turnaround (or inversion), and Δz is the distance traversed by the outward-moving front

	v_o (μm/s)	v_i	t_{inv}	Δz
Dope A ($n = 3$)	16 ± 6.6	4.9 ± 2.5	8.6 ± 4 s	65 ± 6 μm
Dope B ($n = 4$)	39 ± 16	6.1 ± 2.3	4.7 ± 1	121 ± 28

3.2. Film morphology and precipitation mechanism

The confocal backscattering technique does not provide direct evidence regarding the mechanism of precipitation and film formation. On contact with the non-solvent bath, the surface composition of the film becomes tied to the binodal phase boundary (where diffusive driving forces vanish), but layers deeper within the film can cross that boundary, perhaps even reaching into the spinodal region. Film precipitation could occur at depth within the film by means of spinodal decomposition, by means of binodal nucleation and growth, or by means of crystallization, since the crystallization phase boundary is also quickly traversed on immersion. An electron micrograph cross-section of a fully precipitated film is shown in Fig. 4. The left of the film shows a dense skin layer of about 20 μm thickness, which is thought to form promptly on immersion into the non-solvent and which apparently does not scatter light well. The crystallite structure of the film is readily apparent, and is indicative of a nucleation and growth mechanism for film formation, via polymer crystallization.

Nunes and Inoue [7] have found, with cellulose acetate films, that nucleation and growth is the dominate membrane formation outside of a moderate range of polymer concentrations (6–25 wt%). Whether a film will develop via a spinodal decomposition mechanism or a nucleation and growth mechanism depends on the compositional trajectory in the phase diagram, and on the temperature and time spent at a given composition [8] as well as on bath hardness [9], with softer baths favoring the nucleation and growth mechanism. The nylon films studied here are also able to undergo a crystallization transition; calculations of the compositional trajectory show that this crystallization boundary is crossed well before *either* the binodal or spinodal lines are crossed [5]. The scattering results reported here, combined with electron microscopy of the fully formed films, indicates that these nylon films form through crystallization that is nucleated at a depth of more than 60 μm. For the first few seconds after nucleation, the scattering front expands in both directions (toward the bath and toward the substrate). This result is at odds with the substrate-directed front moving with $\sqrt{t}$ dependence reported by McHugh and Tsay [10], yet McKelvey and Koros note that such $\sqrt{t}$ behavior is to be expected only from spinodally decomposing systems [6].

Table 3
Effect of bath hardness, Dope A

	v_o	v_i	t_{inv}	Δz
H_2O ($n = 3$)	16±6.6 μm/s	4.9±2.5	8.6±4 s	65±6 μm
80:20 H_2O/CH_2OOH ($n = 2$)	9.3±4.6	2.0±0.1	14±7	63±24
60:40 H_2O/CH_2OOH ($n = 2$)	2.3±1.0	2.5±1.7	22[a]	28±8.8

[a] One of the two films observed inverted outside of the microscope field of view.

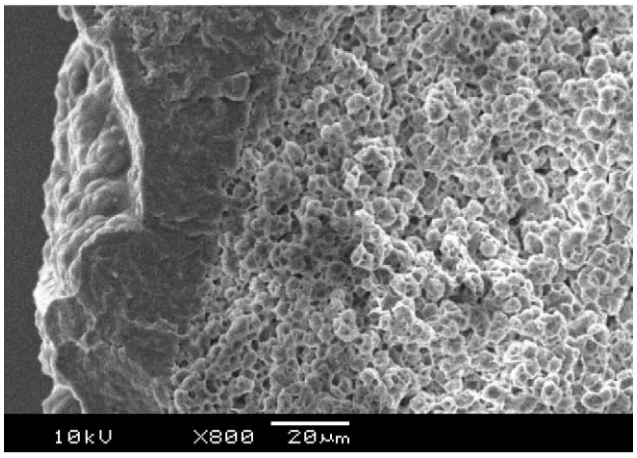

Fig. 4. An electron micrograph of a film (dope A) precipitated in slope-casting chamber B into a hard (pure water) bath. The surface of the film is at left, and is dense and relatively homogeneous. Though this surface skin may form rapidly upon immersion, it would not be expected to scatter a significant amount of light. Deeper within the film are spherical crystallites; this region of the film is clearly heterogeneous and will consequently scatter light well.

The remarkable result that scattering is first observed deep within the precipitating nylon film demonstrates the complexity of the film formation process. Rates of crystallization (when that is the mechanism of film formation) may depend greatly on kinematic factors, such as local viscosity, as well as on thermodynamic factors, such as the composition and compositional 'distance' from the crystallization phase boundary. It appears likely that surface layers of the film fail to initiate crystallization owing to a greater dehydration and vitrification, while deeper layers maintain sufficient water to permit polymer mobility. Further light may be shed on these issues by means of small angle light scattering (which can distinguish spinodal decomposition from nucleation and growth [11]) or though microscopy experiments with fluorescently labeled polymers [12].

4. Conclusions

These measurements demonstrate that confocal backscattering microscopy is a useful tool for the study of polymer precipitation kinetics. With nylon 6 membranes, we have found: (1) the inward velocity of the precipitation front does not differ substantially for low and moderate water content solvents (on immersion into a hard non-solvent), (2) the precipitation initially occurs at some depth (60 + μm) within the film, rather than at the non-solvent interface, (3) the water content in the *solvent* does affect the velocity of precipitation fronts observed from the bath side, with higher water content causing faster front motion and more rapid turnaround, and (4) softer non-solvent immersion baths slow the process, as expected. In electron micrographs, both crystalline and skin regions of the precipitated film were clearly seen.

The large variation in the kinetic parameters from film to film may be caused by the uncontrolled immersion velocity in these experiments, which could affect the early transport of water and formic acid near the film surface. Clearly, future work will aim at improving this aspect of the experimental procedure.

References

[1] Bulte AMW, Folkers B, Mulder M, Smolders C. J Appl Polym Sci 1993;50:13–26.
[2] Cheng L-P, Dwan A-H, Gryte CC. J Polym Sci, B: Polym Phys 1995;33:223–35.
[3] Rajadhyakstra M, Grossman M, Esterowitz D, Webb RH, Anderson R. J Invest Dermatol 1995;104:946–52.
[4] Keith C, Bird G, Farmer M. BioTechniques 1998;25:858–66.
[5] Shih C-H. Mechanism of microporous hollow fiber membrane formation by isothermal precipitation of semicrystalline polymers from solution. Chem Engng 2001;250.
[6] McKelvey S, Koros W. J Membrane Sci 1996;112:29–39.
[7] Nunes S, Inoue T. J Membrane Sci 1996;111:93–103.
[8] Barth C, Gonçalves M, Pires A, Roeder J, Wolf B. J Membrane Sci 2000;169:287–99.
[9] Kim J, Lee H, Kim S. J Membrane Sci 1999;163:159–66.
[10] McHugh A, Tsay C. J Appl Polym Sci 1992;46:2011.
[11] Maugey J, Van Nuland T, Navard P. Polymer 2001;42:4353–66.
[12] Jinnai H, Nishikawa Y, Morimoto H, Koga T, Hashimoto T. Langmuir 2000;16:4380–93.